CHALMERS
UNIVERSITY OF TECHNOLOGY

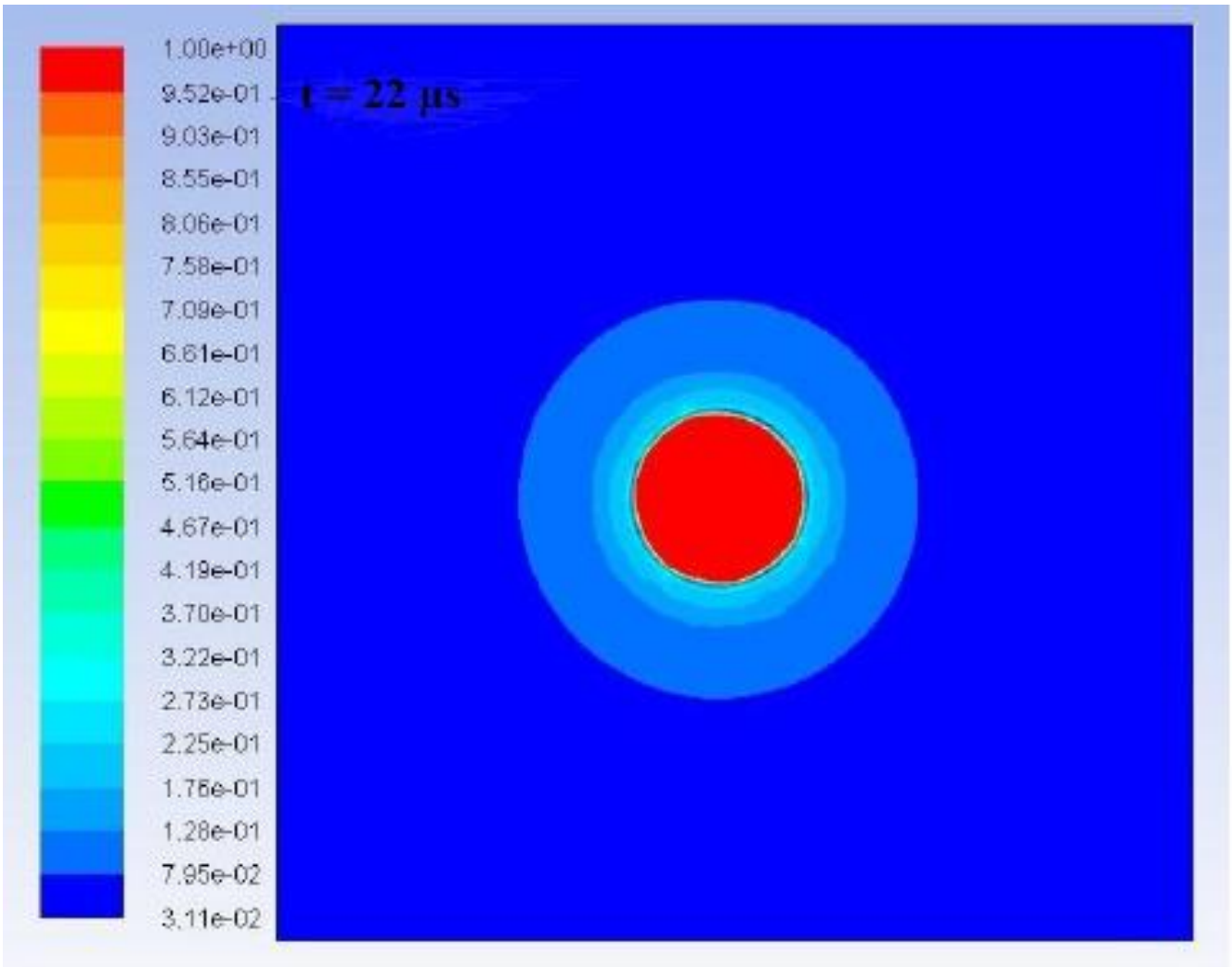

New generation of industrial crystallizers

Numerical simulation of a bubble growth induced by laser

MOHAMMAD GHEISI

Department of Applied Mechanics
CHALMERS UNIVERSITY OF TECHNOLOGY
Gothenburg, Sweden 2015

Abstract

Production of crystals of different chemicals with the desired properties is a not trivial task and great number of studies have been carried out in order to understand the crystallization kinetics. Notwithstanding all these efforts, further investigation is needed to understand the underlying physics and the sequence of events that leads to crystallization. Moreover, introduction of novel technologies that facilitate the crystallization process and, as a result, produces crystals with the desired and controlled quality are essential.

In this thesis, several technologies such as the laser-induced crystallization, ultrasound-induced crystallization, air-lift crystallization, oscillatory baffled crystallization and the high-gravity crystallizer have been studied and their main features are presented. In particular, the study focuses on the laser-induced crystallization or, more specifically, on the growth of a bubble that is induced by laser irradiation in an aqueous solution of ammonium sulfate. The numerical part of study is based on the volume of fluid (VOF) framework and the Schnerr and Sauer cavitation model (G.H.Schnerr, A.J.Sauer, F.I.C.M.F, 2001) to model the bubble growth. The simulations consider mass and energy transfer during the phase change in a stagnant ammonium solution. The simulation results show that the mass fraction of ammonium sulfate increases as a result of evaporation of solvent from liquid into the bubble. The increase of solute concentration during the expansion of a bubble is recognized as a driving force for nucleation. In the same time, it also increases the probability of formation of stable clusters.. The predicted values for the bubble radius as a function of flow time are found to be lower than the experimental data and the maximum predicted bubble radius is higher than the maximum bubble size in another sudy (A. Soare et.al, *Cryst. Growth Des*, 2011).

Acknowledgements

I want to thank my supervisors Professor Srdjan Sasic and Adjunct Professor Oleg Pajalic from Perstrop Company for all their help, patience, support and constructive discussions during the work of this thesis. I also want to thank the Assistant professor Henrik Ström for his help with writing UDF for simulation.

Moreover, I would like to express my gratitude to my father, brother and to the spirit of my passed-away mother for being next to me for my entire studies.

Nomenclature

Latin symbols

ΔC concentration difference

C solute concentration

Cs equilibrium concentration

S relative supersaturation

U flow velocity

g gravity acceleration

F surface tension force

k turbulence kinetic energy

S mass transfer due to evaporation

R_b bubble radius

P pressure

Y_i mass fraction of species i

$\vec{J_\iota}$ diffusion flux of species i

R_i net production due to chemical reaction

S_i mass source term for species i

Greek symbols

σ surface tension

∅ volume fraction or color function

ρ density

μ dynamic viscosity

α volume fraction

ω specific dissipation rate

ν_T turbulence viscosity

β^* closure coefficient

σ_ω closure coefficient

β closure coefficient

σ_k closure coefficient

ν_l kinematic viscosity of liquid

E mass-averaged energy

k_{eff} effective thermal conductivity

S_h energy source term

m mass flux at the interface

h_{lg} latent heat of phase change per kilogram

Subscripts

1 phase one

2 phase two

v vapor

l liquid

b bubble

q phase

Contents

Abstract ... **iii**
Acknowledgements ... **iv**
Nomenclature ... **v**
1 Introduction ... **1**
2 Objective and method of thesis ... **2**
3 Crystallization Kinetics ... **3**
3.1 Primary nucleation ... 4
3.2 Secondary nucleation ... 4
3.3 Crystal growth ... 4
3.4 Crystal morphology ... 5
4 Crystallization methods ... **5**
5 New technologies for crystallization ... **6**
5.1 Oscillatory baffled crystallizer ... 6
5.2 Ultrasound crystallization ... 7
5.3 Laser-induced crystallization ... 8
5.4 Gassing technology ... 10
5.5 Air-lift crystallizer ... 10
5.6 High-gravity Crystallizer ... 11
6 Selection criteria of crystallization technology ... **12**
7 Numerical simulation of the crystallization process ... **13**
7.1 Macroscopic simulation of crystallizers ... 13
7.2 Microscopic simulation ... 14
7.3 Scope of the simulation ... 15
7.4 Volume of fluid ... 15
7.5 Surface tension ... 15
7.6 Momentum equation ... 16
7.7 Physical properties ... 16
7.8 Turbulence modeling ... 17
7.9 Bubble growth model ... 17
7.10 S*chnerr* and *Sauer* cavitation model properties ... 18
7.11 Species transport equations ... 18
7.12 Energy equation ... 19
7.13 Simulation setup ... 19
7.14 Geometrical configuration ... 20
8 Results and discussion ... **22**
9 Conclusion ... **26**
10 Future work ... **26**
References ... **27**

1 Introduction

Crystallization from a solution is a common separation and purification process. Crystallization is a solid-fluid separation process in which crystals are formed from a homogenous solution. Crystallization has been utilized for many decades and it is today widely used in industries such as pharmaceutical, fine chemicals, food and material industries. The aqueous or organic solvents are used to create solutions and crystallization can be performed by cooling, salting out, reaction, evaporation. For example, addition of a second solvent can reduce solubility and result in crystallization in processes like the watering-out, salting-out or precipitation [1]. The main purpose of crystallization is production of crystals with a set of desired properties, e.g. a narrow crystal size distribution (CSD), an acceptable morphology, maximum crystal purity and high yield. The priority of one feature over the other mainly depends on type of the product. For example, the purity of crystal is a most important feature in pharmaceutical industry, whilst in production of fertilizers, the purity of a product is less significant [2].

When a solute dissolves beyond its equilibrium concentration, the solution becomes supersaturated which is a driving force for crystallization. Supersaturation has a significant influence on all properties of a crystal, such as purity, shape, size etc. Several challenges are encountered when it comes to the unit operation of crystallization. The operation conditions such as the cooling rate, feed flow rate, feed concentration and evaporation rate have important effects on the produced crystals and finding an optimum operating conditions is not trivial. Additionally, a simultaneous heat and mass transfer that is influenced by the fluid and particle mechanics is another challenge during the design and process control of a crystallizer. Moreover, crystallization deals with multicomponent, multiphase systems whose crystal mean size and CSD vary with time. The solution concentration has temporal changes which directly have an effect on the crystal nucleation and growth [2] [3].

One of the difficulties during crystallization is how to avoid primary nucleation which has a significant effect on the CSD and mean size of the product. One way to control primary nucleation is seeding by which secondary nucleation is induced and the CSD can be controlled. Seeding is basically an addition of previously produced crystals to the solution. Seeding can create difficulties in sterile processes and additional regularity efforts in the pharmaceutical processes. The biopharmaceutics classification system (BCS) class II drugs are sparingly water soluble and reduction in crystal size down to micro/nanometer in order to increase bioavailability is necessary [4]. In order to overcome the problems mentioned above, the introduction of novel technologies such as ultrasound or laser-induced crystallization is considered vital [5].

The stirred crystallizer is one of the common types of industrial crystallizer and minimization of secondary nucleation is a demand in stirred vessels due to the high shear stress creation of the impeller. Air-mixed devices could be a promising alternative for the stirred vessel and can enhance the crystal quality and suppress secondary nucleation [6]. The crystal size distribution (CSD) has an important role in production of crystals with the high quality and the efficiency of downstream unit operations such as filtration and washing. The CSD is under the influence of the primary nucleation and crystal growth during the crystallization process. The implementation of a novel crystallization technology that can control the primary nucleation is necessary in order to produce the crystal with desirable specifications [7].

2 Objective and method of thesis

Crystallization is a technology in which a single or multiple components are separated in form of crystals from a homogeneous system or solution. The purpose of crystallization is typically purification of a substance or getting a product in an in-demand form. For those purposes, specifications are to be met through well-defined properties of crystals (e.g. purity, shape, size, etc.). At present, crystallization is probably the major separation and purification technique for production of pharmaceutical products and micro/nano size chemicals. A great number of heavily coupled phenomena are a part of the crystallization process, such as nucleation, growth and agglomeration of crystals among others. To be able to meet the desired specifications for final products, it is of great importance to control the crystallization process.

There are two main objectives in this thesis: i) to look at novel and promising crystallization technologies, characterized by different driving forces, that typically target a certain part (or sub process) within the process of crystallization and ii) to increase our theoretical and modelling understanding of the relevant underlying mechanisms connected with the induction of nucleation by a method chosen in objective i.

A theoretical and a computational study have been performed aiming at describing the expansion of a bubble as a part of formation of crystals and their consequent growth. Special attention will be paid to evaporation of the solvent and its effects on bubble dynamics and formation of crystals. The available literature suggests that there exists a thin zone at the interface of a bubble in which the dissolved substance from the core of the bubble is stored. It is believed that most of the fundamental phenomena included in the process of crystallization take place in this zone. For the planned studies, a comprehensive simulation technique will be used. The technique is based on the Volume of Fluid (VOF) multiphase simulation framework. The steps in thesis are summarized and depicted in Fig.1.

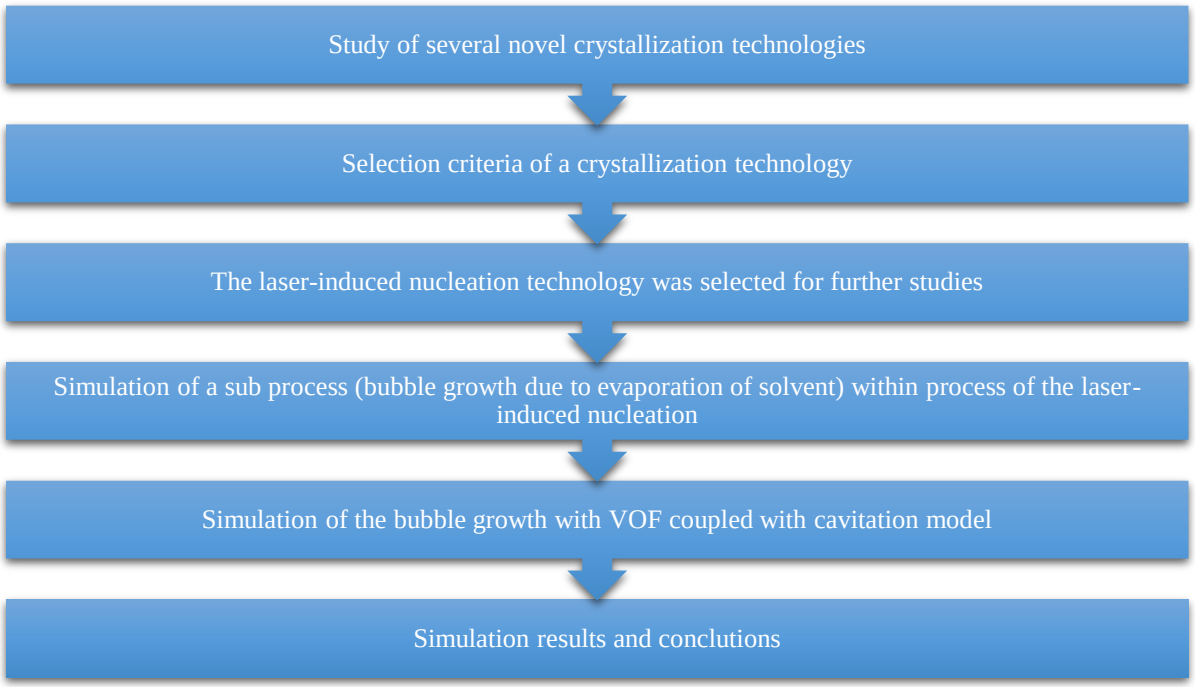

Fig.1. Steps in the thesis.

3 Crystallization Kinetics

Crystallization involves the following stages: nucleation, mass transfer of solute to the surface of crystal and incorporation of solute in the crystal lattice. The crystallization kinetics is governed by supersaturation. The supersaturation is excess amount of solute that is dissolved beyond the equilibrium concentration in a solvent at a given temperature. The supersaturation is created by cooling that is shown with a green line in Fig.1 or evaporation that is shown with a blue line in the same figure, or by adding a second solvent [2]. The supersaturation can be expressed in the form of a difference between the solution concentration C and the equilibrium concentration Cs:

$\Delta C = C - Cs,$

or as a relative ratio:

$S = \frac{C}{Cs}$ $\sigma = 1 - S.$

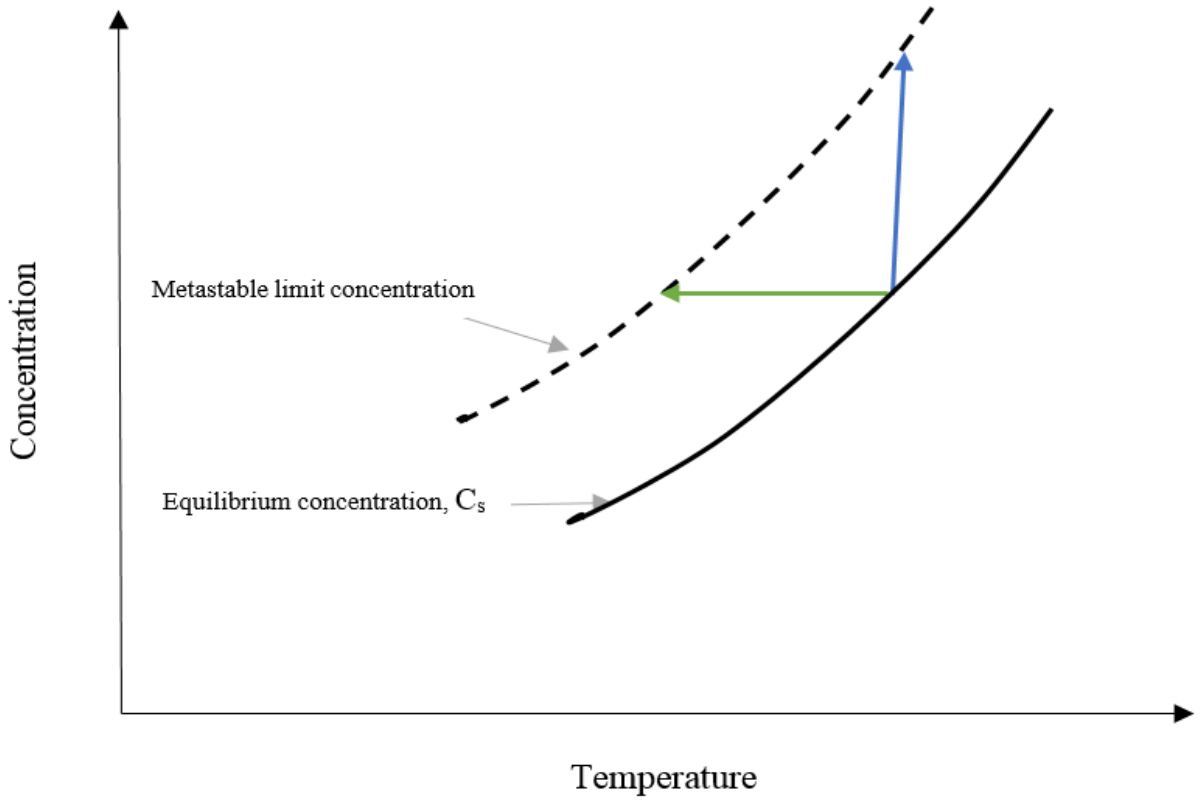

Fig. 2. Representative solubility curve

As it is shown in Fig.2, the solid curve represents the equilibrium concentration of a solute below which the solution is unsaturated. If the saturated solution is cooled or evaporated up to a certain concentration through a green or blue line respectively, the solution is still clear and no nucleation occurs. The maximum value of supersaturation that solute-solvent system can

handle is a metastable zone with (MZW). The saturation temperature, solvent type, presence of impurities, crystalline seeds and the cooling rate determine the extent of the MZW.

The seed crystals start to grow within the metastable region to release the supersaturation and the concentration reaches to any point at the equilibrium solubility curve. A continuation of the evaporation or cooling has a maximum at which spontaneous nucleation takes place (dashed line) and a large amount of tiny crystals will be produced, a process that is termed primary nucleation. If nucleation occurs at the presence of a crystalline surface, it then is termed secondary nucleation. The selection of a technique for reaching supersaturation depends on the product purity, the thermodynamic and physical properties of the solute and solvent and, of course, on economic considerations. For chemicals with less sensitive solubility to the temperature, the evaporation technique is a reasonable technique. The cooling technique is applied once solubility of the solute changes significantly with temperature variation [2] [3].

3.1 Primary nucleation

The primary nucleation can be either homogeneous or heterogeneous. The former type of nucleation occurs in the absence of impurities e.g. dust and/or surface of crystallizer equipment. On the other hand, the heterogeneous nucleation occurs in the presence of impurities and/or surface of crystallizer equipment e.g. impeller, pump, wall of tank, etc. The heterogeneous nucleation needs less energy for nucleation than does the homogeneous nucleation since the presence of a foreign surface reduces the formation energy of a stable cluster [3]. The heterogeneous nucleation is common in many industrial applications and it is unlikely to find the homogeneous nucleation in chemical processes.

3.2 Secondary nucleation

The secondary nucleation frequently occurs in industrial crystallizers and it refers to nucleation in the presence of crystals of a material that is being crystallized in the supersaturated solution. In 1968 Strickland and Constable [3] proposed several mechanisms for secondary nucleation such as, initial breeding (crystal dust sweep off a newly introduced seed crystals), needle breeding (the detachment of weak out-growth), polycrystalline breeding (the fragmentation of a weak polycrystalline mass), and the collision breeding (a complex process resulting from interaction of crystals with one another or with parts of the vessel). The contact breeding (attrition) is the most likely mechanism for secondary nucleation. The presence of a crystal surface causes the nucleation at a lower supersaturation in comparison to the primary nucleation. Hence, seeding the supersaturated solution is the most common method to control crystal mean size and CSD [3].

3.3 Crystal growth

There are several theories that have been developed to describe the crystal growth: surface energy theories, adsorption layer theories, kinematic theories and diffusion-reaction theories (critical reviews by Wells (1946), Buckley (1952), Strickland-Constable (1968), Lewis (1980), Chernov (1980, 1989) and Nvvlt et al. (1985). According to diffusion-reaction theories, there

are two steps by which the crystal grows. First, there is a mass transport of solute from bulk of solution to the stagnant film adjacent to the adsorption layer. Second, we may have a first order reaction (integration) that leads to attachment of the solute molecules into the crystal lattice at the adsorption layer. The driving forces for both steps are concentration gradients. The rate of diffusion and reaction steps can vary from face to face of the crystal. However, if crystal growth is a diffusion- or reaction-controlled process, it is possible to predict the growth rate with the expression that is proposed by Mullin [3].

3.4 Crystal morphology

Crystals are categorized by their shapes. According to *Law of Constant Interfacial Angles* proposed by *Hauy* in 1784, the angles between crystal faces, for a typical compound, are constant even if the size and shape of crystals are different. Mullin also suggested that a large crystal consists of many small units with an identical shape. This notion led to concept of space lattice. Bravais [1] has shown that there are only 14 space lattices. There are substances that form the crystal with different structures by which crystal possess different physical properties. A crystal with various lattice structures is called a polymorph [2].

4 Crystallization methods

As mentioned before, the supersaturation is the driving force for crystallization. With respect to the way by which supersaturation is created, different crystallization methods exist. Melt crystallization [1] creates the supersaturation by cooling the melt below the melting point of the mixture. There are four methods to produce crystals from a solution. Cooling a solution that decreases the solubility of a solute is a common method for crystallization. This method is effective when the solubility curve is a strong function of the temperature. Evaporation is another method by which the solute concentration increases and it leads to formation of crystals. The evaporation method is suitable when the solubility curve changes slightly or is constant as a function of temperature. Precipitation, understood as a chemical reaction between two reactants that yields a product with a very low solubility, is a fast method for crystallization. Finally, the crystallization with addition of an anti-solvent is another method by which the addition of a second solvent decreases the solubility of the solute in the solution that leads to creation of crystals [2] [1].

5 New technologies for crystallization

In this section several novel crystallization technologies are studied. Previous studies and experiments regarding the discussed technologies are presented. The results and conclusions of previous studies are given with respect to the crystallization technologies.

5.1 Oscillatory baffled crystallizer

The continuous oscillatory baffled crystallizer (COBC) is a tubular crystallizer with periodic orifice baffles with oscillatory motion in addition to the net flow. As flow passes through baffles, vortices are produced that enhance radial mixing and introduce plug flow along the column. According to a recent study, this technology has several advantages listed below [8];

- A significant reduction of operation time compared with conventional stirred tank crystallizers.
- Perfect mixing along the crystallizer due to a repeated creation of eddies.
- Production of high cooling rate that is uniform and controllable.
- Control crystal size, crystal size distribution and morphology by changing concentration, cooling rate, oscillation frequency and amplitude (e.g. the higher oscillation amplitude and frequency, the smaller is the crystal size).
- Holding time has no significant effects on crystal size distribution (CSD) that implies reduction in process time.
- Capability of production of desired morphology.
- Lower capital cost for COBC than a batch process.
- Provide safety through a simple process and a much lower inventory of raw material and products.
- Lower energy consumption and waste generation.
- Linear scale-up of equipment.

5.2 Ultrasound crystallization

Liquid anti-solvent crystallization generally consists of mixing of solution with an anti-solvent and precipitation of crystals. Crystallization with a T-mixer ensures uniform mixing with no supersaturation gradient. The process becomes precipitation-controlled and results in a uniform nucleation rate with a narrow CSD in a continuous mode operation. According to the study by Beck El.al [4], a T-mixer was used to mix anti-solvent with solution of active pharmaceutical ingredient (API) in order to generate uniform supersaturation. The nucleation rate was improved by the presence of sonication which reduces the metastable zone width through generation of a pressure gradient and significant reduction in characteristic mixing time by changing mass transfer mechanism and therefore preventing crystal growth.

As mentioned before, the process is precipitation-controlled, which means that the crystal size can be controlled by using different stabilizers [4]. According to a patent, ultrasound crystallization causes a sono-chemical reaction and produces free radicals that can damage unsaturated oil [9]. A new hypothesis based on the segregation of liquid mixture by inducing pressure gradient, namely the pressure diffusion theory, by ultrasound was investigated. It was concluded that the cavitation bubble acts as a cluster attachment that causes the medium size clusters around the bubbles to aggregate and that it pushes away the large clusters in order to increase the nucleation rate [10].

Certain amount of energy must be irradiated to initiate primary nucleation by ultrasound (US). In addition, there is a region below which the ultrasonic irradiation hinders primary nucleation. It was also observed that ultrasound irradiation did not affect perfection of crystal shapes at a low irradiation time and low supersaturation. Moreover, the final crystal size is controlled by number of initial nuclei [11] [7]. A reduction in the induction time is reported due to a higher diffusion rate once ultrasound is irradiated. A dramatically low agglomeration and change in crystal pattern are reported as ultrasound is introduced to the crystallization of roxithromycin [12]. The Mean Chord Length (MCL) and particle mean size (PMS) both increase by increasing the induction period, while MCL and MPS are reduced by decreasing the induction period. The number of crystals produced at a low ultrasonic energy is lower due to the fact that the number of nuclei that overcome a critical free energy is smaller in primary nucleation stage. On the other hand, the number of final crystals increases by increasing the ultrasonic energy because of the enhancement effect of ultrasonication.

Nevertheless, there is a practical limit for ultrasound irradiation when the primary nucleation becomes unstable as the higher amount of ultrasonic energy is applied [7]. Polymorphism control is another challenge encountered when a crystal has a possibility to form different polymorphs, especially if the metastable polymorph is desirable. A control of L-Glutamic acid polymorphs via reactive crystallization by inducing ultrasound and seeding of controlled supersaturation was accomplished [13]. A reduction in the induction time and a narrow crystal size distribution are reported. Moreover, it is found that the cavitator design, input power and physical properties of a solute have influence on the number of nuclei. There is no relationship between the induction time and the insonication period. An easily soluble compound has larger mean size crystals compared to partially soluble compounds.

The nucleation rate is collapse pressure-dependent as long as this pressure is below the pressure which forms nuclei of the critical size of a single molecule [14]. An increase in the nucleation rate, lowering supersaturation limit and modification of the growth of some crystal faces make

the reduction in the mean crystal size, higher mass fraction recovered and change in crystal faces [15]. Without utilizing ultrasound, the induction time decreases as the supersaturation rises and induction of ultrasound reduces induction time dramatically for all supersaturation ratios. According to the authors [14], ultrasound enhances diffusion and it is the reason for a much lower induction time compared to crystallization without sonication. In addition, a sharp CSD, reduced metastable zone width (MZW) and higher nucleation rate were observed in the experiments [16].

Production of nano and micro crystal that rise bioavailability and are favored by the pharmaceutical industry are achieved when US is induced [16]. Once the amount of ultrasound energy absorbed by the solution (Calorimetric power) increases, the MZW reduces. Calorimetric power is frequency dependent so that the amount of energy absorbed by the solution is different at different input frequencies. An increase in supersaturation enhances nucleation and crystal growth up to a certain level and further increase of supersaturation ratio decreases nucleation because of the diffusive transport and integration reaction limitations. It is concluded that there is also an optimum supersaturation ratio when the CSD is narrow without reduction of the crystal mean size [5].

5.3 Laser-induced crystallization

There are two methods of laser-induced crystallization: the photochemical and the non-photochemical one. In the former type, a high energy laser causes a reaction and the product of this reaction acts as a nucleation center. The photochemical method can be with and without cavitation. The one without cavitation involves accumulation and/or orientation of molecules to create nuclei. The applied techniques have an influence on morphology and the induction time. This means that it might take from minutes to days without cavitation and from nanoseconds to minutes with cavitation to achieve nucleation. According to previous studies, crystallization occurs at a threshold energy (or higher) of the formation of a cavitation bubble. In addition, an increase in the supersaturation reduces this threshold. The size of a bubble is related to the power of laser irradiation and evaporation has a significant effect on crystallization. It was also observed that the nucleation rate is influenced by supersaturation and laser power. In a recent study, nucleation and crystal growth were modeled in the way that the evaporation of solvent causes accumulation of solute in the interface of a bubble that this is a driving force for nucleation and crystal growth. The bubble dynamics and nucleation were modeled as a function of laser power, initial supersaturation, duration of laser irradiation and properties of the solution [17].

A single pulse near-infrared laser light was applied to produce KCl crystals. The laser pulse improves nucleation through an isotropic electronic polarization of a subcritical cluster of solute and reduces the free-energy of the nuclei. It was shown that the crystallization yield depends on the supersaturation and the input power of laser, whereas nucleation has a threshold power below which nucleation does not occur. Presence of impurities can either reduce or enhance laser-induced nucleation. The dependence of KCl nucleation on polarization of laser was examined and no evidence of polarization effect was found [18].

The same fraction of samples were nucleated in the presence of a both short and long pulse width near infrared laser light. It was shown that crystallization efficiency depends on the peak

power density of the laser and not on the duration and total energy of the laser pulses. Two mechanisms are proposed for KCl crystallization: during the presence of an electric field, the solute tends to be absorbed by the existing subcritical clusters to enlarge the cluster in the way that it reaches a stable critical size as the electric field disappears; or, the presence of an electronic field manipulates the structure of the subcritical clusters that might be of a liquid-like to a more crystalline structure [19].

The laser-induced nucleation of the gas bubble for the aqueous solution of sucrose saturated with CO2 gas is studied. The number of bubbles produced per nanosecond pulses has a quadratic dependence on the laser power and there is a threshold for laser power below which no bubble is formed. It was found that there were no bubbles formed for femtosecond pluses and the reason might be lower energy densities per pulse of femtosecond pulses in comparison to nanosecond pulses. It was also observed that the number of bubbles rises linearly with sucrose concentration and that the bubbles decrease significantly if the carbonated solution is filtered prior to laser irradiation. A simple model was proposed to describe bubble nucleation and growth [20].

A laser-induced nucleation for materials with different properties (e.g. molecular weight, solvent, additives, etc.) has been reported. The femtosecond laser-induced nucleation has some advantages over the nanosecond one, including higher efficiency, versatility and induction of nucleation without aging of supersaturation solution and nucleation at lower supersaturation concentrations. It was concluded that nucleation occurs as a result of the cavitation bubble formation either for protein or small organic compounds. According to another experiment mentioned in this article, evaporation of solvent creates a cavitation bubble and condensation of solute or precipitant in the vicinity of the bubble surface promotes the nucleation.

Laser ablation of irregular shape protein crystal was performed and high quality macro seed was produced. The laser-processed crystal was seeded in a supersaturation solution and a lager crystal with high quality was obtained. The laser-induced nucleation is a non-contact technique in contrast with ultrasound nucleation in which transducers must be in contact with the solution to be able to produce focused ultrasonic waves. Therefore, utilizing a laser-induced technique does not need large modifications in a conventional crystallization process [21].

The nucleation mechanism consist of two steps: first, solute molecules join together to form a liquid-like structure. Second, the clusters rearrange the structure to form nuclei with an ordered structure. The second step is proceeding faster due to the Kerr effect that is induced by the electric field of the laser irradiation. According to their nonphotochemical laser-induced nucleation (NPLIN) experiment, laser irradiation leads to a dramatically increased nucleation rate. The shortest mixing time of lysozyme solution with precipitant solution, higher peak intensities and shorter pulse durations promote NPLIN efficiency [22].

Based on another research study, there is vapor inside a bubble produced in a laser-induced technique, whereas in ultrasound cavitation there is a gas bubble. Therefore, the bubble dynamics of the former one are governed by evaporation, condensation and thermal diffusion that are much faster than the mass transfer and it is not suitable to consider an equilibrium bubble size. No relation between the laser energy absorbed by a solution and the radius of a crystal ring was found. The authors believe that crystal nuclei are formed directly after the bubble formation and, as bubble expands, the crystals move outward and continuously gain

mass and inertia. This means that their movement becomes more decoupled from the movement of the interface.

Therefore, when the bubble implodes, the crystal ring remains in its position. Moreover, KMnO4 crystals were not formed by a single laser pulse for supersaturated solution below 7% but after several irradiations of the laser pulses crystals were detected. But for the supersaturation higher than 7%, crystals are formed with a single laser pulse. The reason is that most of the laser energy is consumed to cause the local temperature rise of the solution which decreases the supersaturation. Thus, no sufficient amount of energy remains to be spent for evaporation of the solvent in order to compensate thermal effects - therefore nucleation will not occur. As several pulses have irradiated, after each collapse the local temperature rises in such a way that, for subsequent pluses, more energy is spent to increase evaporation which, in turn, promotes supersaturation and eventually nucleation takes place. The MZW and the solubility curve importance are illustrated by selecting two different chemicals with various MZW and solubility curves so that their effects are reflected in the amount of crystals. It is believed that an optical disturbance is due to nucleation that can be detected by the change in the refractive index. The difference between the characteristics and the sequence of events in cavitation induced by ultrasound and laser was also mentioned [23].

5.4 Gassing technology

Two possible hypotheses for effect of bubbles on nucleation during batch cooling crystallization were examined by replacing a cavitation bubble with a gas bubble: first, the evaporation of the solvent into a bubble that increases the solute concentration at the bubble interface in order to facilitate the nucleation. Second, the reduction of nucleation energy by presence of the bubble surface that acts as a foreign particle. A gas bubble expands during its life time whilst a cavitation bubble formed in ultrasound induced crystallization expands and then collapses to create a high local pressure and temperature. According to figures provided in this experiment, a reduction in MZW occurs in all solutions which conveys reduction in the induction time. Gassing time and saturation of the synthetic air were shown no influence on the MZW. Therefore, the increase of supersaturation due to evaporation of solvent into the bubble has no effect on nucleation. As a consequence, heterogeneous nucleation seems to be the reason for nucleation. Moreover, while different bubble surfaces do not influence induction time, the presence of gas causes nucleation to occur at a lower supersaturation ratio as in the ultrasound crystallization [24].

5.5 Air-lift crystallizer

An air-lift crystallizer utilizes air flow for circulation and mixing of a solution, which, in turn, impedes secondary nucleation. As a consequence, reduction of attrition and breakage of crystals occur. Crystal quality is improved due to reduction of the surface shear and prevention of secondary nucleation. Moreover, the crystal size is controllable by manipulating the sparger, air flow rate and disengagement zone. For example, a lower air flow rate results in a narrower crystal size distribution and larger crystals with better shape and quality [17]. In another study, an increase in the air flow rate increases both the gas- and the crystal hold-up and causes air

bubbles circulation. To prevent air bubble circulation and to be able to increase the air flow rate, insertion of a disengagement zone to the crystallizer is necessary.

A higher air flow rate increases liquid circulation and mass transfer to the crystal and, at the same time, provides a uniform temperature field and prevents supersaturation gradients [25]. According to experimental studies, a shorter residence time when oscillatory baffled crystallizer or tubular crystallizer is used, is reported. Thus, when a longer residence time is desirable, utilizing CBOs or the tubular crystallizer with excessive length creates several problems for instance, high pressure drop and risk of scaling as result of large surface area [6].

5.6 High-gravity Crystallizer

A rotating packed-bed reactor was designed to generate an acceleration higher than the gravitational acceleration on the Earth. The experimental results have shown that the mean size of CaCO3 particles can be controlled and adjusted in the range of 17-36 nm through the change of operation conditions such as the high-gravity levels, fluid flow rates, and the reactant concentrations. The crystal structures of these compounds synthesized in high-gravity conditions were the same as those in the gravitational conditions. The high-gravity reactive precipitation (HGRP) technology is believed to be able to produce nanoparticles with a low cost and high-volume production. Therefore it has potential applications in industry. In this method, the characteristic mixing time is lower than the corresponding reaction time that under such condition a uniform nucleation and crystal growth occur in the entire reactor [26].

6 Selection criteria of crystallization technology

In this thesis, a need for further studying of the laser-induced crystallization is identified due to a number of reasons. The equipment for the laser-induced technique implies a lower maintenance cost due to its non-contact nature compared to the conventional crystallization processes and to the rotating equipment used in the high-gravity crystallizer. The capability to control the crystal structure (polymorph) by simply changing the laser polarization that facilitates production of crystals with a desired polymorph is an important feature of this technology. From a scientific point of view, creation of a single cavitation bubble makes it easier to study in detail the fundamental physics for the nucleation and crystal growth. In addition, the primary nucleation and number of nuclei which are important steps in the crystallization process can be controlled by utilizing laser irradiation. According to [17], laser irradiation with 10 KHz pulse repetition can produce around $2.2.10^5$ crystals with the random number of crystals between 10 and 40 per each laser pulse that shows the capability of a high volume production. The same study also mentioned that a laser with high power is applied in welding and drilling industry with 10 to 60 joule per pulse. Thus, the laser equipment for crystallization application that needs only up to 5mJ per pulse is already readily available.

7 Numerical simulation of the crystallization process

A turbulent multiphase flow contains a wide range of spatial and temporal scales. This implies that the scope of information and extension of the details about the flow behavior can be divided into several ranges, such as microscopic, macroscopic etc. Depending on the level of information that is needed and the size of the domain of interest, the scale of a simulation is selected. It is worth mentioning that the microscopic simulation gives more details about the flow behavior with the cost of a higher computational effort in comparison to the macroscopic simulation. Thus, there is always a trade-off between a computational cost and the level of information about the fluid behavior. Since macroscopic simulations are computationally affordable with the currently available computer power, it is a more desirable scale for preforming numerical simulations in an industrial scale.

7.1 Macroscopic simulations of crystallizers

The crystal growth is controlled by fluid dynamic conditions around the crystals. The behavior of crystals in the downstream unit operations is governed by the product CSD that is directly connected with the crystal growth. Moreover, spatial variation of the supersaturation is up to a great extent related to the macromixing and to the mean and turbulent flow field. In order to have rational design, understanding of kinetics of the nucleation, crystal growth and agglomeration and breakage rates are vital. Further, these phenomena are strongly coupled by the local concentration and hence the flow field. Thus, the computational fluid dynamics (CFD) simulation coupled with the population balance modeling (PBM) and discrete particle modeling (DPM), is a suitable choice in order to predict the CSD and study the macromixing and flow pattern in the entire crystallizer. Ultimately, a better control of the crystallization process is achievable in different industrial crystallizers [27].

Beck et.al [4] investigated the effect of different parameters on ultrasound-induced crystallization through an experiment with batch crystallizers. The authors concluded that the degree of mixing and the flow pattern have a strong influence on the number of produced crystals. Thus, further CFD simulations that take into account the ultrasound or laser effect, in order to optimize the crystallizer parameters, would be beneficial [28]. The CFD-PBE (PBE is population balance equation that is applied wherever the interaction between a large number of particles is studied) simulation in an Eulerian framework is applied to predict the full CSD in a precipitation batch reactor. The nucleation, growth and agglomeration are to be taken into account by appropriate models. The same study [28] did a qualitative analysis and quantitative comparison with experimental results. Jingcai Cheng et.al [29] studied the capture of a bimodal distribution size and calculation of the agglomeration rate for different particle sizes. Their simulation results can be useful for some novel processes such as nanoparticle production.

The strategies of how to scale-up the crystallizer and how to develop a new process via CFD simulation and a process system engineering software, are proposed by Wei [30]. In order to account for an anisotropic flow field during crystallization process in a crystallizer, a coupled simulation of the crystallization and fluid dynamics was performed. Besides, since the crystallization occurs in macro-scale and fluid dynamics occurs in micro-scale, the scale integration methods are also applied at the study work of Kulikov Et al. [31]. A coupled CFD-PBE-PDF (probability density function) simulation was performed in order to study the mixing

effect of anti-solvent on an agitated semi-batch crystallizer. The influence of agitation speed, addition mode and scale-up on primary nucleation, size-dependent growth and the CSD and dissolution rate were numerically examined [32].

The coupled CFD-PBE was utilized to model the crystallization process in an impinging jet crystallizer. The studies have shown the effect of a jet Reynolds number on the degree of inhomogeneity, supersaturation, nucleation and the growth rate [33]. Chew Et al. [34] studied the dynamical fluid patterns for both impeller-driven batch crystallizer and oscillatory baffled batch crystallizer by utilizing CFD. The same group also did experiments with both crystallizers to observe the differences between the obtained crystals. Ali Et al. [35] Investigated the crystal dynamics by taking into account the collisions with the impeller, walls of reactor and baffles to be able to model the attrition and secondary nucleation. The same study applied a coupled CFD-DEM (discrete element modeling) simulation in a Lagrangian framework.

7.2 Microscopic simulations of crystallizers

There are several numerical methods for microscopic simulations of multiphase flow. Some of the methods are described briefly here. The interested reader can find more details in given references.

Marker and Cell (MAC) *Method* [36]. In this method a set of massless marker particles located at the interface between a fluid and a free surface is convected by local fluid velocities in order to identify the region occupied by that fluid. In MAC method the marker particles can be utilized to reconstruct the interface location in a fixed grid.

Front Tracking (FT) Method [37]. FT is a more accurate and complex method compared to the MAC method. In this method the interface is tracked explicitly by marker particles that have no mass and they are moved by local fluid velocities (Eulerian velocity fields). The difference between MAC and FT is that the interfaces are tracked by a dynamic grid (Lagrangian frame) which gives a more accurate position of the interface but the complexity rises from how the interface grid interact with the fixed grid.

Level Set (LS) Method [38]. In this method a distance function that includes information about the distance of a numerical cell to the interface is defined and it is convected by the local fluid velocity. The interface is indicated as a zero level set of that distance function.

Volume of Fluid (VOF) Method. The volume of fluid (VOF) is an Eulerian model that tracks the interface between the phases. In this method a region (volume) adjacent to the interface instead of the interface itself is tracked by solving a transport equation for a function. The function (color function/volume fraction) is defined in the way that it has the value of unity in a region occupied by fluid and zero where there is no fluid. If the volume fraction in a certain cell is between zero and one, that cell contains the interface. The average of color function indicates a field that has information about the volume fraction of one of the phases in a computational cell and this field is transported by the local fluid velocity. In VOF there are some difficulties with the accurate estimation of the curvature of the interface and reconstruction of the interface between neighborhood cells. Nevertheless, VOF is a reliable method for simulation of a single bubble or very few bubbles since it resolves accurately the interface between fluids. The transport equation for VOF is given in section 7.4.

7.3 Scope of the simulation

After selecting the technology, the decision should be made about identification of the part of the laser-induced nucleation that leads to crystallization. There are several restrictions here for the simulation of bubble dynamics. First, it is not trivial to simulate the creation of a bubble. Second, a very fast creation of the bubble immediately after laser irradiation makes it that the temperature drops from 230 ºC to 120 ºC and the bubble radius reaches to the size of 350µm within only a few nanoseconds. Third, it is not possible to simulate the crystal formation from a solution in the vicinity of the bubble surface. Fourth, the simulation of the creation, expansion and collapse of the bubble is complex and time-consuming. Therefore, with respect to these four restrictions, it is decided to model the bubble expansion when the bubble and solution have approximately a constant temperature of 120 ºC and 130 ºC, respectively and the bubble reaches the maximum radius of 600 µm within about 50 µs according to experimental data in reference [17].

7.4 Volume of fluid

The VOF consists of an advection equation for predicting the orientation and location of the interface as shown in equation (1) where u is the velocity and $\emptyset$ is the volume fraction or color function at the discrete level. Volume function is unity if cell is filled with phase one and is zero if the cell is filled with phase two. Most of the VOF algorithms use second order discretization scheme in time and higher order discretization scheme on the flux form in space to update the volume fraction. The fractional step or operator split method is utilized to move the interface in on direction at a time in most of the CFD codes [39].

$$\emptyset_t + u.\nabla\emptyset = 0. \qquad (1)$$

The volume fraction equation may be solved by the implicit or explicit time discretization scheme. In the explicit scheme the value of any variable at time step *n+1* is calculated as a function of the value of that variable at time step *n*. In an implicit scheme, the estimation of any variable at time step *n+1* is calculated as a function of that value at the same time step. .

The implicit scheme was selected for discretization of the volume fraction due to limitation imposed by the Schnerr and Sauer [40] cavitation model that is not compatible with the explicit scheme. The Schnerr and Sauer model is applied in this thesis in order to model the bubble growth, and it is discussed in more details in section 7.9. The compressive discretization scheme was set for the volume fraction which is a second-order accurate scheme. The implicit scheme does not have the Courant number limitation and thus a large time step can be used. On the other hand, the numerical diffusion of the interface is pronounced, something that can cause a less accurate solution. To suppress the numerical diffusion imposed by the implicit scheme, a very low time step of 2.5e-7 s, 400 iterations per time step and the refinement of the mesh have been applied.

7.5 Modelling of Surface tension

To model bubble dynamics, it is necessary to add a source term for the surface tension in the Navier-Stokes momentum equation. Note that all other terms in that equation act continuously over the volume except the surface tension term that acts only at the interface. A possible way to solve this problem is to use the continuum surface force technique (CSF) [41]. The CSF

considers the surface tension force as a body force which is active in a small fluid region around the interface. As a consequence of the local variation of the CSF, the unphysical currents close to the interface could be generated in the numerical simulation – those currents are termed "parasitic" currents. In other words, parasitic currents are induced when the pressure gradient term cannot be balanced by the surface tension force in the momentum equation due to the variation of the surface tension in directions other than radial direction. A high magnitude of these parasitic currents can destroy the interface. Therefore, special attention should be given to mitigate or possibly prevent parasitic currents [42]. ,

7.6 Momentum equation

A single momentum equation is solved for the entire domain and there is a source term for surface tension (F) in the cells that are shared with both phase as follow:

$$\frac{\partial U_i}{\partial t} + U_j \frac{\partial U_i}{x_j} = -\frac{1}{\rho}\frac{\partial P}{\partial x_i} + \nu \frac{\partial}{\partial x_i}\left(\frac{\partial U_i}{\partial x_j} + \frac{\partial U_j}{\partial x_i}\right) + g_i + F \, . \quad (2)$$

The momentum equation is a function of the volume fraction through ρ and ν that are averaged properties based on the volume of phases in each cell. The surface tension is modeled based on continuum surface force (CSF) model as follow:

$$F = (\sigma k \hat{n} + \nabla_s \sigma)\delta, \quad (3)$$

where σ is surface tension coefficient, k mean interfacial curvature and ∇_s delta function. The first term in the equation acts in the normal direction and the second term acts in the tangential direction. As the equation expresses, if the surface tension coefficient is constant then the tangential term is zero.

7.7 Physical properties

Since the solution is a multi-component mixture, the volume-weighted mixing law has been selected to calculate the density of the solution as a function of composition. As the pressure in the bubble is above the standard pressure, the assumption of an ideal gas for the vapor phase is not a suitable choice. On the other hand, the variation of a local relative pressure is small. In order to maintain stability of simulations and reproduction of comparable results with the previous studies, the incompressible ideal gas has been selected to estimate the density based on the operating pressure and the local temperature. Due to the constant temperature during the expansion period of the bubble, the heat capacity, viscosity, thermal conductivity have been set to constant values with respect to the temperature of the phases. The full multicomponent diffusion has been activated and a constant value for diffusion coefficient of the solute chosen for the diffusion of ammonium sulfate in water. The material properties appearing in the transport equations are volume-fraction averaged properties. For example, the density is given by equation (4) when the second phase is tracked.

$$\rho = \alpha_2 \rho_2 + (1 - \alpha_2)\rho_1 \quad , \quad (4)$$

where α is volume fraction and subscripts 1 and 2 are the phases.

7.8 Turbulence modeling

The standard k-ω model which is a two-equation model was selected to model turbulence. In this model the specific dissipation (ω) is proportional to the turbulent kinetic energy (k) and turbulent dissipation (ε) and it is inverse of timescale on which dissipation occurs. The transport equation for the specific dissipation is given by

$$\frac{\partial \omega}{\partial t} + \langle U_j \rangle \frac{\partial \omega}{\partial x_j} = \alpha \frac{\omega}{k} \nu_T \left[\left(\frac{\partial \langle U_i \rangle}{\partial x_j} + \frac{\partial \langle U_j \rangle}{\partial x_i} \right) \frac{\partial \langle U_i \rangle}{\partial x_j} \right] - \beta^* \omega^2 + \frac{\partial}{\partial x_j} \left[\left(\nu + \frac{\nu_T}{\sigma_\omega} \right) \frac{\partial k}{\partial x_j} \right], \quad (5)$$

and the transport equation for the turbulence kinetic energy is given by

$$\frac{\partial k}{\partial t} + \langle U_j \rangle \frac{\partial k}{\partial x_j} = \nu_T \left[\left(\frac{\partial \langle U_i \rangle}{\partial x_j} + \frac{\partial \langle U_j \rangle}{\partial x_i} \right) \frac{\partial \langle U_i \rangle}{\partial x_j} \right] - \beta k \omega + \frac{\partial}{\partial x_j} \left[\left(\nu + \frac{\nu_T}{\sigma_k} \right) \frac{\partial k}{\partial x_j} \right] , \quad (6)$$

here the turbulent viscosity is calculated by $\nu_T = \frac{k}{\omega}$, ν is the kinematic viscosity and α, β^*, σ_ω, β, σ_k are closure coefficients. The standard k-ω model is implemented with the low Reynolds corrections and turbulence damping options. The low Reynolds correction option suppresses the turbulence viscosity in regions where the flow has a low Reynolds number. The turbulence damping option is necessary since it is desirable to dampen the turbulence close to the interface to keep the integrity of the bubble and also the high velocity gradient at the interface is needed to be dampened in order to model the flow in that region correctly. Moreover, the k-ω model does not need the wall function to predict the flow field near the wall correctly. In order to minimize the excessive production of turbulence in the vicinity of stagnant region, the production limiter option for the turbulence model was activated [43].

7.9 Bubble growth model

The bubble growth were modeled based on the Schnerr and Sauer cavitation model. The cavitation model is in accordance to the Rayleigh-Plesset equation that comprehensively describes the bubble dynamics. The model comprises the exact expression for the net mass transport from the liquid to vapor via the vapor volume fraction equation as follows:

$$\frac{\partial}{\partial t}(\alpha \rho_v) + \nabla . \left(\alpha \rho_v \vec{V} \right) = \frac{\rho_v \rho_l}{\rho} \frac{D\alpha}{Dt} , \quad (7)$$

$$S = \frac{\rho_v \rho_l}{\rho} \frac{D\alpha}{Dt} , \quad (8)$$

where α is the vapor volume fraction, R is the net mass transfer due to the evaporation and condensation. ρ_v, ρ_l, n_b and ρ are vapor, liquid, and mixture densities, respectively. The volume fraction is related to the bubble radius and the number of bubbles per unit volume of the liquid as follow:

$$\alpha = \frac{n_b \frac{4}{3} \pi R_B^3}{1 + n_b \frac{4}{3} \pi R_B^3} , \quad (9)$$

Here, R is modeled according to the Raylieght-Plesset equation which describes the growth of a single bubble given by

$$R_b \frac{d^2 R_b}{dt^2} + \frac{3}{2}\left(\frac{dR_b}{dt}\right)^2 = \left(\frac{P_v - P}{\rho_l}\right) - \frac{4v_l}{R_b}\frac{dR_b}{dt} - \frac{2\sigma}{\rho_l R_b}, \quad (10)$$

where R_b is the radius of bubble, σ is surface tension, ρ_l is the liquid density, P_v is the bubble surface pressure and P is the local far-field pressure.

It is assumed that the interface velocity is constant during bubble growth and the first term on the right- hand side of the equation (10) is zero. As the contribution of the viscous and surface tension terms are small compared to the pressure term, the former terms were neglected and the equation (10) is simplified to the equation (11) as follows:

$$\frac{dR_b}{dt} = \sqrt{\frac{2}{3}\frac{P_v - P}{\rho_l}} \ . \quad (11)$$

By combining equations (9), (10), (11), the following expression is derived:

$$R = \frac{\rho_v \rho_l}{\rho}\alpha(1-\alpha)\frac{3}{R_B}\sqrt{\frac{2}{3}\frac{(P_v - P)}{\rho_l}} \ , \quad (12)$$

where $P_v$the pressure inside the bubble and P is the far-field pressure of the liquid. P_v is set to the saturation pressure of vapor in the absence of mass transfer, dissolved gases and viscous damping. If $P_v \geq$ P then mass transfer from liquid to the bubble due to the evaporation occurs and if $P_v <$ P then, the mass transfer from the vapor to liquid due to the condensation occurs. Therefore, the saturation pressure has been set in the way that only the evaporation occurs and the interface velocity is roughly equal to the velocity of the bubble during the expansion in the experiment. The model accommodates the saturation pressure correction due to the local value of turbulence pressure fluctuations [40].

7.10 Schnerr and Sauer cavitation model properties

The cavitation model is not compatible with explicit VOF in ANSYS Fluent. The cavitation model can be applied to the single liquid and Fluent cannot simulate multiple cavitation processes. The Schnerr and Sauer model does not take into account the effect of non-condensable gases. The model is numerically robust and is expected to converge fast. The model generally does not need any specific initial conditions and itis applicable to both mixture and Eulerian multiphase models. The cavitation model is compatible both with pressure-based segregated and coupled solvers in ANSYS Fluent. It is good to mention that the evaporation and condensation model were also coupled with VOF to simulate the bubble growth but it did not give a desirable results

7.11 Species transport equations

The species transport equations were solved for the chemical species presented in the system to obtain the mass fraction of the species as shown in equation (13) where Y_i is the mass fraction

for the i^{th}species, $R_i$is the production of species i, S_i is the source term that is the evaporation in this simulation, $\vec{J_i}$ transport of species *i* by diffusion.

$$\frac{\partial}{\partial t}(\rho Y_i) + \nabla \cdot \left(\rho \vec{V} Y_i\right) = -\nabla \cdot \vec{J_i} + R_i + S_i. \quad (13)$$

7.12 Energy equation

The energy equation is shared between phases and is given by

$$\frac{\partial}{\partial t}(\rho E) + \nabla \cdot \left(\vec{v}(\rho E + P)\right) = \nabla \cdot \left(k_{eff} \nabla T\right) + S_h. \quad (14)$$

The VOF model treats energy, E, and temperature, T, as the mass-averaged variables:

$$E = \frac{\sum_{q=1}^{n} \alpha_q \rho_q E_q}{\sum_{q=1}^{n} \alpha_q \rho_q} \ , \quad (15)$$

where E_q for each phase is calculated based on the specific heat of that phase and the shared temperature, ρ and k_{eff} are the shared density and effective thermal conductivity, respectively, and S_h is the source term due to the phase change that is a multiplication of the mass flux at the interface (m) and the latent heat of phase change per kilogram (h_{lg}) as

$$S_h = m.h_{lg} \ . \quad (16)$$

7.13 Simulation setup

The simulation is performed with a transient pressure-based solver. The implicit VOF and the standard k-ω model are set for multiphase and turbulence models, respectively. The energy and species equations are solved as well. The liquid phase with the properties of an aqueous ammonium sulfate solution of 75 gr per 100 gr of water at 130 ºC and vapor phase with properties of water vapor at 120 ºC are defined. The models for interaction between phases as a result of the surface tension and mass transfer are set to the CSF model and cavitation model, respectively.

As mentioned before, the Shnerr and Sauer model is set for the mass transfer mechanism. In order to increase the accuracy of solution, the spatial numerical scheme for the momentum, turbulent kinetic energy, specific dissipation rate, species and the energy equations are set to QUICK. PISO is selected for the pressure velocity-coupling that is recommended for the transient flow calculations. PISO is the most robust pressure velocity- coupling scheme and is faster than the SIMPLE and SIMPLER schemes. The PRESTO! Scheme is set for the pressure equation that is recommended for VOF simulations. Since the implicit VOF was applied, the geometric reconstruction scheme is not available/compatible for the volume fraction equation. Thus, the compressive discretization scheme which has high accuracy is chosen for the volume fraction.

7.14 Geometrical configuration

As illustrated in Fig. 3. The geometry consist of two walls that are labeled with letter C and D. These walls consider as glass wall with no slip condition at the constant temperature. In the simulation the heat capacity is also set to the heat capacity of glass. The other two boundaries namely A and B was set to symmetry boundaries. The reasons are that they are far enough from the bubble interface (region of interest) and there was no sufficient information about these boundaries in the experiment setup which was conducted in reference 17. The computation domain and boundaries are shown in Fig.2. A 2D square solution domain with X=Y=3000µm and circle with a 350µm radius represent the geometry. The initial size of the bubble is selected according to the section 7.3. The interior of the rectangle is defined as the ammonium sulfate solution.

All the properties of both vapor and liquid phases including viscosity, density, heat capacity, etc. were extracted from chemical handbooks at the corresponding temperature of each phase.

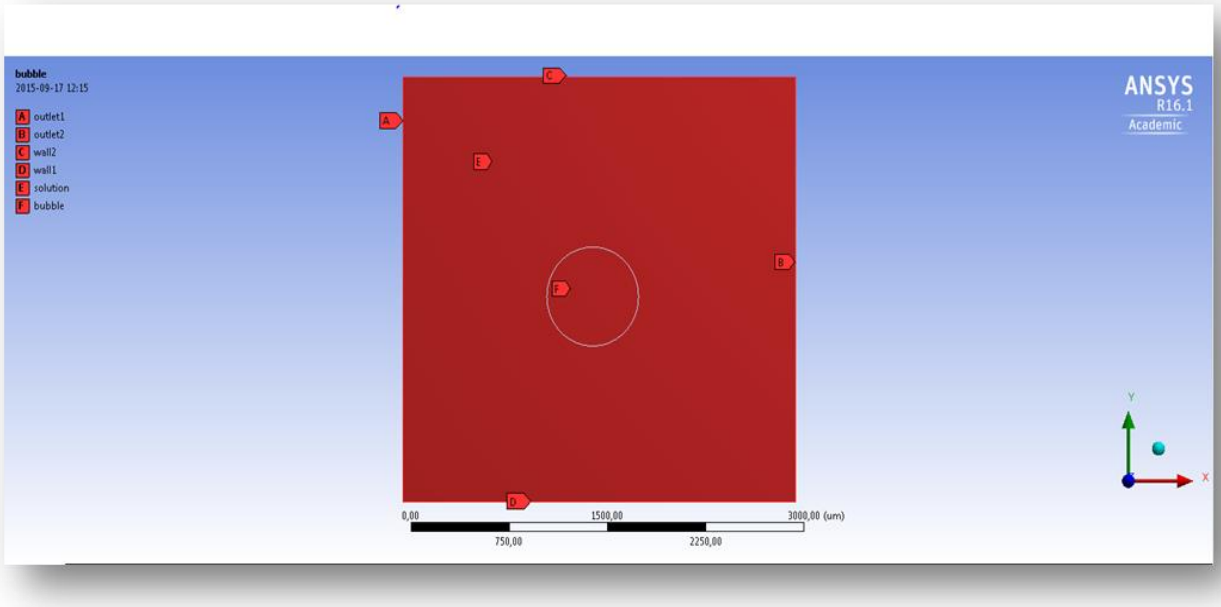

Fig. 3. Diagram of the solution between two glass walls

The number of cells per diameter of the bubble is around 64 and the total number of cells before mesh adaption is 10116 as illustrated in Fig.3 the number of cells after adoption with the gradient of vapor volume fraction is 39900 cells.

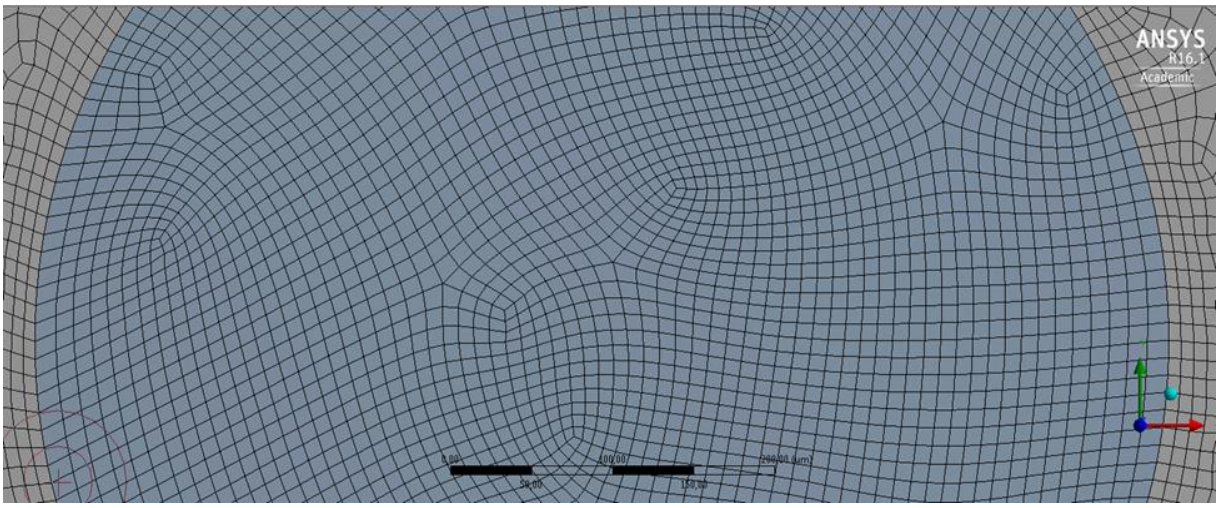

Fig. 4. Mesh resolution, the light blue part represents the bubble and the gray part represents the solution

The maximum skewness is 0.36 which is below the maximum value of 0.95. The maximum aspect ratio is 4.7 which is below the maximum value of 5. A very fine mesh is generated in order to minimize the numerical error imposed by the first-order accurate VOF and CSF models.

8 Results and discussion

Fig. 4 illustrates the change of the ammonium sulfate mass fraction as a function of the flow time. The curve indicates the slight increase in the mass fraction of the solute from 0.428 to the 0.4286 due to the evaporation of water. The increase of solute concentration during the expansion of the bubble is a driving force for the formation of clusters and it also rises the probability of formation of the clusters that have exceeded the critical size. Since the presence of a foreign surface reduces the formation energy of a stable cluster, it can be concluded that the chance of formation of nuclei in the vicinity of the bubble surface is much higher than in the bulk solution. Therefore, the ring of crystals is formed adjacent to the bubble surface in the laser-induced nucleation experiment after a few seconds.

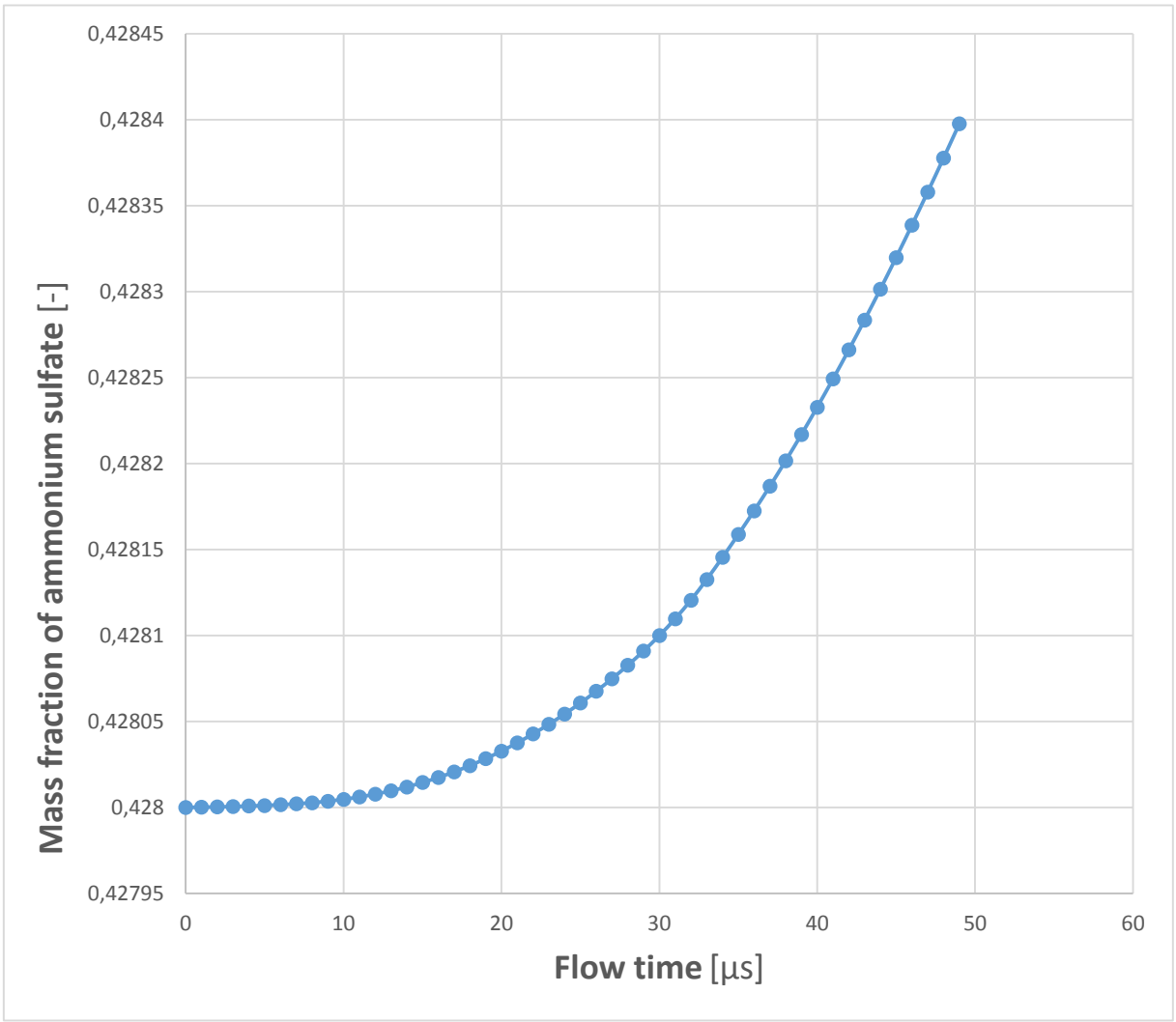

Fig 5. The mass fraction of ammonium sulfate versus flow time

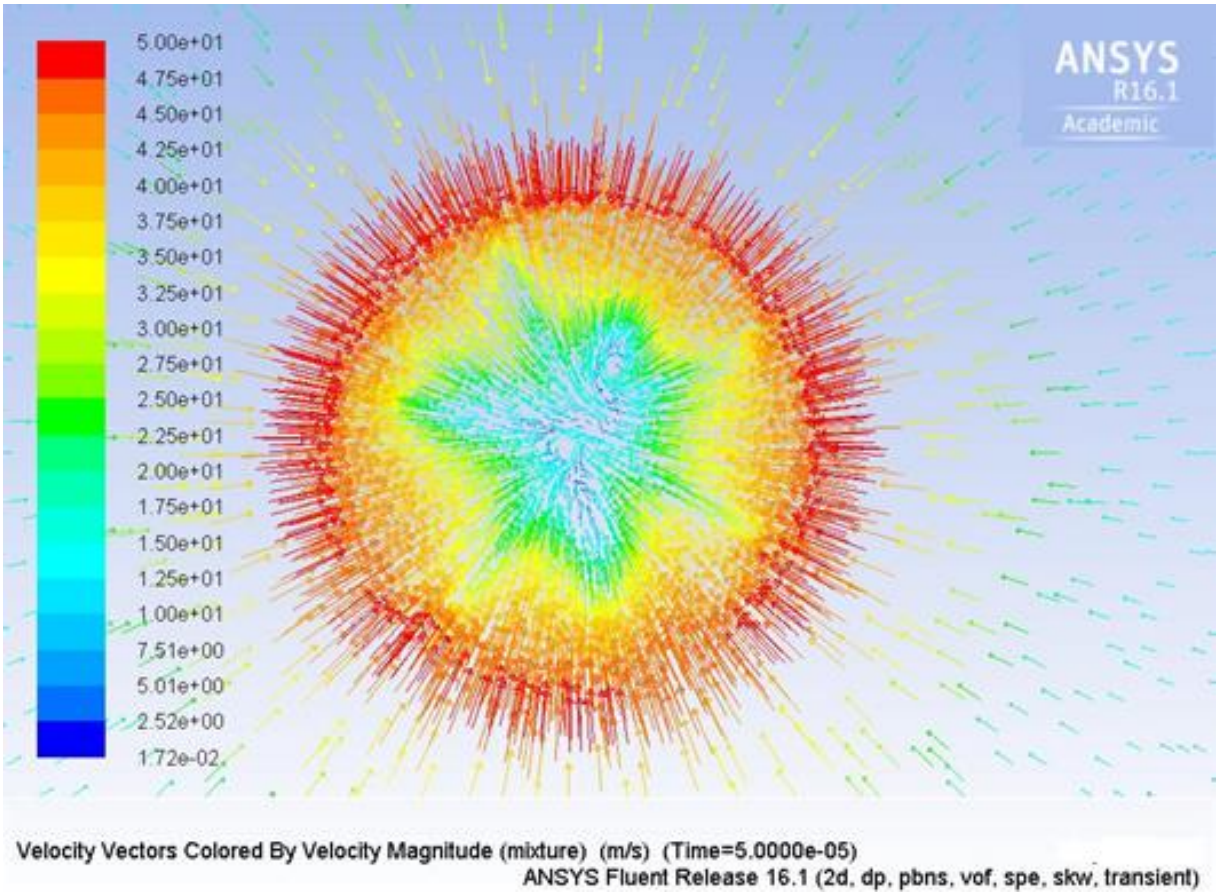

Fig. 6. The velocity vector around and inside the bubble at 50μs

Fig. 5. shows the velocity vector at the 50 μs after expansion of the bubble. As Fig. 5 indicates, the velocity is directed towards the center of the bubble. The reason behind this observation is that the mass transfer takes place from the liquid to the vapor phase. The highest velocity is observed at the vicinity of the interface. The implementation of the k-ω model dampens the turbulence close to the bubble and, as expected, keeps the integrity of the bubble during the expansion. No references or previous studies about the velocity magnitude have been found to be able to compare or possibly validate the velocity magnitude around the bubble interface.

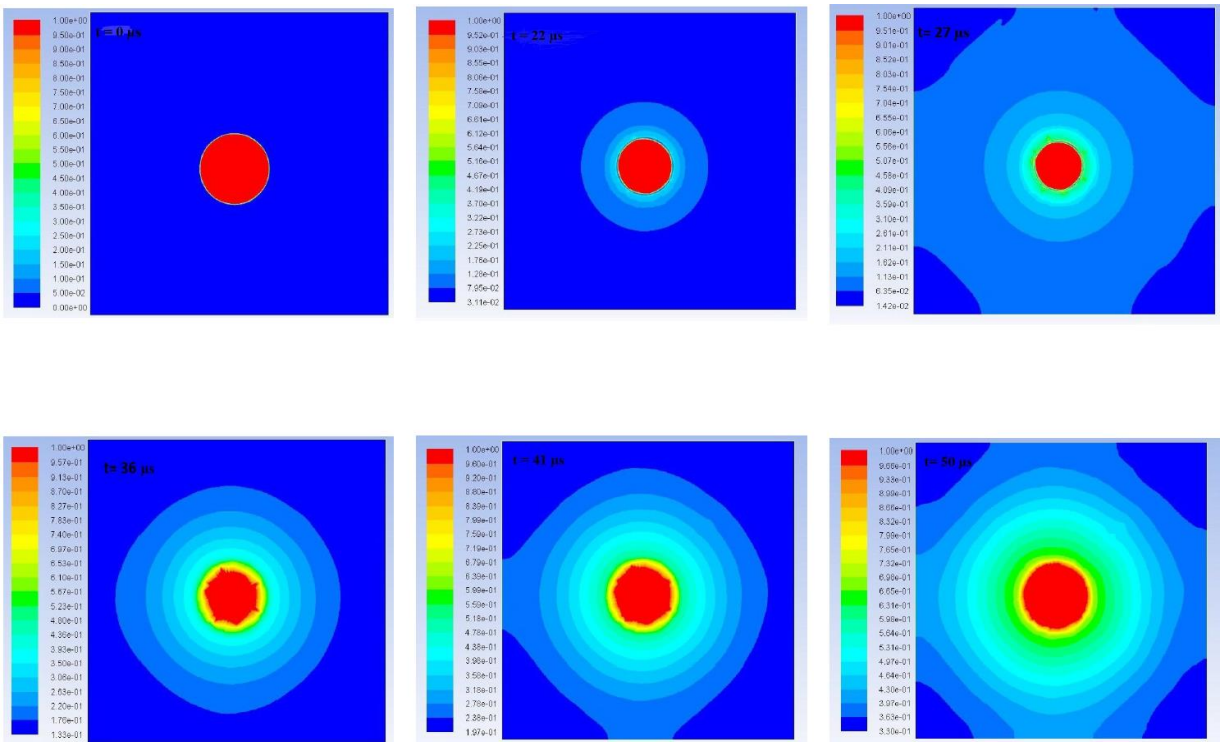

Fig. 7. Evaluation of the vapor volume fraction within 50 µs

Fig. 6 shows the bubble growth within 50 µs. Numerical diffusion around the bubble interface is observed and also cavitation formation in those cells around the bubble that have pressure below the saturation pressure. The accuracy of the simulation is affected by the numerical diffusion and cavitation formation. However, the bubble size as a function of time can be plotted if the bubble is defined as those cells that have vapor volume fraction within a certain range. The definition of the bubble as those cells that have a specific range of volume fractions of the vapor is not trivial. In this study several ranges of the volume fraction of vapor were tried in order to capture the growth of the bubble. Definition of vapor as those cells that have the vapor volume fraction between 0.55 and 1 gave an acceptable prediction of the bubble radius.

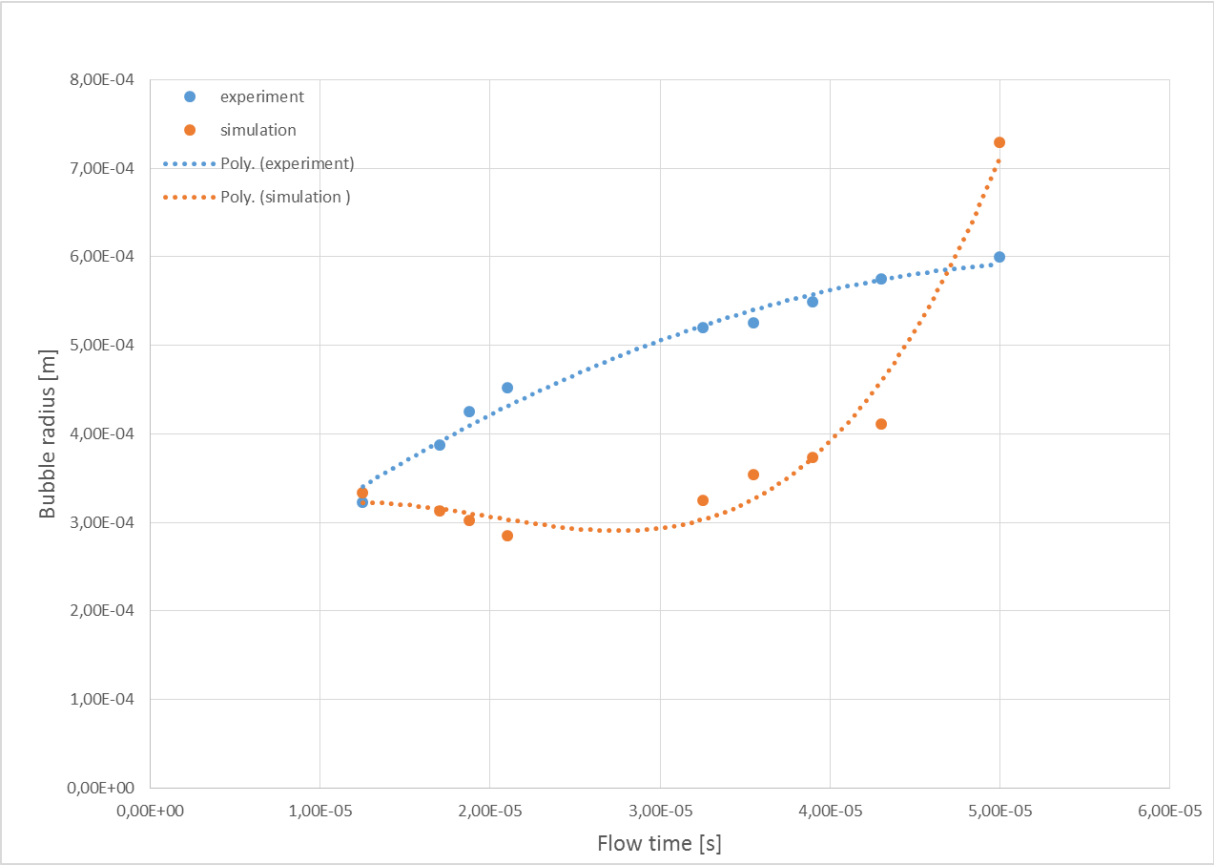

Fig. 8. Comparison between the modeled and the experimentally obtained bubble growth [17]

According to Fig. 7 the predicted bubble radius increases within 50 µs from 350 µm to 729 µm. According to the experimental result presented in [32], the maximum size of the bubble during the expansion for laser power of the 0.27mJ is 630 µm. The comparison of the bubble radius predicted by the simulation with the experimental result [32] indicates that the predicted values are lower than the experimental ones and also, that the maximum predicted bubble radius is higher than the maximum bubble size in the experiment. The reason behind this disagreement may be in the numerical diffusion due to the implicit volume fraction tracking. The ideal gas assumption for the vapor phase is another source of these disagreement. Moreover, we are not able to solve the volume fraction in every iteration to update the volume fraction in every iteration because of applying the implicit VOF. Last but not least, the possibility of formation of the cavitation bubbles in the solution where the vapor pressure falls below the saturation pressure could also smear the prediction of the bubble radius.

9 Conclusion

A number of novel crystallization technologies are studied here. Based on several criteria discussed in the thesis, laser-induced crystallization is selected as a most promising one for future crystallizers. For that reason, this type of crystallization is investigated by numerical simulations. The effect of the bubble growth due to evaporation of a solvent on crystallization in the laser-induced nucleation is modeled. It is found that the increase in the mass fraction of the solute due to evaporation and the presence of the bubble surface are the two main reasons for nucleation. The explanation for the latter statement is through the existence of a ring of detectable crystals exactly at the position of the bubble.

The Schnerr and Sauer cavitation model is used within the VOF framework to model the bubble growth that involves a simultaneous evaporation. It is also shown in the thesis that the velocity is directed towards the center of the bubble (phase change from liquid to the bubble) which implies that the proposed framework is able to simulate the evaporation as the dominant phenomenon during the bubble growth. The disagreement between the simulated value and the experimental result of the bubble diameter may originate from numerical diffusion, the assumption of an ideal gas for the vapor bubble, the incompatibility of the cavitation model with the explicit VOF and the possibility of formation of the cavitation bubbles in the solution where the vapor pressure falls below the saturation pressure.

10 Future work

Investigation of a multiple stage airlift crystallizer in series which has the same volume of a single airlift crystallizer could be a possible future work. Since the resident time is distributed and hence the crystal size distribution would be narrower for multiple configuration than the single air-lift crystallizer of the same volume.

Integration of airlift crystallizer with the laser-induced crystallizer that takes the advantage of both the nucleation rate control of the laser-induced technology and the crystal growth control of the airlift crystallizer. Moreover, the nucleation and growth steps of crystallization can be separated by manipulate the laser power, repetition of laser irradiation, air flow rate and sparger type.

Irradiation of the laser pulses with for example 10 kHz repetition rate to the liquid film that is flowing on an inclined plane. It brings us one step closer to apply laser-induced nucleation technique at the pilot scale or even the industrial scale.

Finding an optimal operating conditions for the gassing technology in order to get narrower CSD would be another possible research work.

The investigation of the crystal growth in an airlift crystallizer with the disengagement zone by utilizing different spargers, air flow rates and crystallizer geometries is also an interesting research work [17].

References

[1] J. D. Seader, E. J. Henley, D. Keith Roper, Separation process principles : chemical and biochemical operations, USA: John Wiley & Sons, Inc., 2011.

[2] A. Mersmann, crystallization technology handbook, USA: Marcel Dekker, Inc., 2001.

[3] J. W. Mullin, Crystallization, 4th Ed., Oxford: Butterworth-Heinemann, 2001.

[4] Christian Beck, Sameer V.Dalvi, RajeshN.Dave, "Controlled liquid antisolvent precipitation using a rapid mixing device," *Chemical Engineering Science,* p. 5669–5675, 2010.

[5] Anna Kordylla, Stephan Koch, Feelly Tumakaka, Gerhard Schembecker, "Towards an optimized crystallization with ultrasound: Effect of solvent properties and ultrasonic process parameters," *Journal of Crystal Growth,* p. 4177–4184, 2008.

[6] Richard Lakerveld, Jeroen J. H. van Krochten, Herman J. M. Kramer, "An Air-Lift Crystallizer Can Suppress Secondary Nucleation at a Higher Supersaturation Compared to a Stirred Crystallizer," *Crystal Growth & Design,* p. 3264−3275, 2014.

[7] Masahiro Kurotani, Etsuko Miyasaka, Satomi Ebihara, Izumi Hirasawa, "Effect of ultrasonic irradiation on the behavior of primary nucleation of amino acids in supersaturated solutions," *Journal of Crystal Growth,* p. 2714–2721, 2009.

[8] Simon Lawton, Gerry Steele, Phil Shering, Lihua Zhao, Ian Laird, Xiong-Wei Ni*, "Continuous Crystallization of Pharmaceuticals Using a Continuous Oscillatory," *Organic Process Research & Development,* p. 1357–1363, 2009.

[9] B. J. Arends, R. A. Blindt and M. Patr, "Crystallization process using ultrasound". EngleWood Cliffs, NJ (US) Patent US006630185B2, 2003.

[10] John Dodds, Fabienne Espitalier,Olivier Louisnard,RomainGrossier,RenéDavid, "The Effect of Ultrasound on Crystallisation-Precipitation Processes: Some Examples and a New Segregation Model," *Inter science,* p. 18–28, 2007.

[11] Etsuko Miyasaka, Yumi Kato, Minoru Hagisawa, Izumi Hirasawa, "Effect of ultrasonic irradiation on the number of acetylsalicylic acid crystals produced under the supersaturated condition and the ability of controlling the final crystal size via primary nucleation," *Journal of Crystal Growth,* p. 324–330, 2006.

[12] Z. Guoa, M. Zhangb, H. Lib, J. Wangb, E. Kougoulos, "Effect of ultrasound on anti-solvent crystallization process," *Journal of Crystal Growth,* p. 555–563, 2005.

[13] Henry Hatakka, Hannu Alatalo, Marjatta Louhi-Kultanen, Ilkka Lassila, Edward Hæggström, "Closed-Loop Control of Reactive Crystallization PART II: Polymorphism Control of L-Glutamic Acid by Sonocrystallization and Seeding," *Chemical enginnering Technology,* p. 751–756, 2010.

[14] C. Vironea, H.J.M. Kramera, G.M. van Rosmalena, A.H. Stoopb, T.W. Bakkerb, "Primary nucleation induced by ultrasonic cavitation," *Crystal Growth,* p. 9–15, 2006.

[15] B. J. Blum, J. H. J. Brooks and M. G. Mortenson, "Methods for controlling crystal growth, crystallization, structures and phases in materials and systems". USA Patent US007972390B2, 2001.

[16] John Sander, Brad W. Zeiger, Kenneth S. Suslick, "Sonocrystallization and sonofragmentation," *Ultrasonics Sonochemistry,* p. 1908–1915, 2014.

[17] Anamaria Soare, "Technologies for Optimisation and Control of Nucleation and Growth for New Generations of Industrial Crystallizers," Delft, The Netherlands, Ipskamp Drukkers, 2014, pp. 40-90.

[18] Andrew J. Alexander, Philip J. Camp, "Single Pulse, Single Crystal Laser-Induced Nucleation of Potassium Chloride," *CRYSTAL GROWTH & DESIGN,* p. 958–963, 2009.

[19] Martin R. Ward a, Iain Ballingall, Matthew L. Costen, Kenneth G. McKendrick, Andrew J. Alexander, "Nanosecond pulse width dependence of nonphotochemical laser-induced nucleation of potassium chloride," *Chemical Physics Letters,* p. 25–28, 2009.

[20] Martin R. Ward, William J. Jamieson, Claire A. Leckey, Andrew J. Alexander, "Laser-induced nucleation of carbon dioxide bubbles," *The Journal of Chemical Physics,* p. 144501, 2015.

[21] Hiroshi Y. Yoshikawa, Ryota Murai, Hiroaki Adachi, Shigeru Sugiyama, Mihoko Maruyama, Yoshinori Takahashi, Kazufumi Takano Hiroyoshi Matsumura, Tsuyoshi Inoue, Satoshi Murakami, Hiroshi Masuhara, Yusuke Mori, "Laser ablation for protein crystal nucleation and seeding," *Royal society of chemistry,* pp. 2147-2158, 2014.

[22] In Sung Lee, James M. B. Evans, Deniz Erdemir, Alfred Y. Lee, Bruce A. Garetz, Allan S. Myerson, "Nonphotochemical Laser Induced Nucleation of Hen Egg White Lysozyme Crystals," *Crystal Growth & Design,* p. 4255–4261, 2008.

[23] Anamaria Soare, Rory Dijkink, Marcos Rodriguez Pascual, Chao Sun, Peter W. Cains, Detlef Lohse, Andrzej I. Stankiewicz, and Herman J. M. Kramer, "Crystal Nucleation by Laser-Induced Cavitation," *Crystal Growth & Design,* p. 2311–2316, 2011.

[24] Kerstin Wohlgemutha, AnnaKordyllaa,1, FeellyRuetherb, GerhardSchembeckera, "Experimental study of the effect of bubbles on nucleation during batch cooling crystallization," *Chemical EngineeringScience,* pp. 4155--4163, 2009.

[25] Anamaria Soare, Sergio A. Pérez Escobar, Andrzej I. Stankiewicz, Marcos Rodriguez Pascual,, "2-D Flow and Temperature Measurements in a Multiphase Airlift Crystallizer," *Industrial and chemistry research,* 2013.

[26] Jian-Feng Chen, Yu-Hong Wang, Fen Guo, Xin-Ming Wang, Chong Zheng, "Synthesis of Nanoparticles with Novel Technology: High-Gravity Reactive Precipitation," *Ind. Eng. Chem. Res.,* pp. 948-954, 2000.

[27] Chinmay V. Rane, Arijit A. Ganguli, Ekambara Kalekudithi, Raosaheb N. Patil, Jyeshtharaj B. Joshi1, "CFD Simulation and Comparison of Industrial Crystallizers," *THE Canadian Journal of Chamical Engineering,* p. 92, 2014.

[28] Graaf, Jeroen van der, "Nucleation of ammonium sulfate and alfa-lactose monohydrate due to ultrasonic irradiation," Delft University of Technology, faculty of Applied sciences, Delft, 2011.

[29] Jingcai Cheng, ChaoYang, Zai-ShaMao, "CFD-PBE simulation of premixed continuous precipitation incorporating nucleation,growth and aggregation in a stirred tank with multi-class method," Chemical Engineering Science, 469–480, 2012.

[30] Wei, Hong-yuan, "Computer-aided design and scale-up of crystallization processes: Integrating approaches and case studies," chemical engineering research and design, 1377–1380, 2010.

[31] V. Kulikov, H. Briesen, W. Marquardt, "Scale integration for the coupled simulation of crystallization and fluid dynamics," *Chemical Engineering Research and Design*, p. 706–717, 2005.

[32] Xing Yi Woo, Reginald B. H. Tan, Pui Shan Chow, Richard D. Braatz, "Simulation of Mixing Effects in Antisolvent Crystallization Using a Coupled CFD-PDF-PBE Approach," *Crystal Growth & Design, Vol. 6, No. 6,*, pp. 1291-1303, 2006.

[33] Xing Yi Woo, Reginald B. H. Tan, Richard D. Braatz, "Modeling and Computational Fluid Dynamics-Population Balance Equation-Micromixing Simulation of Impinging Jet Crystallizers," *Crystal Growth & Design*, p. 156–164, 2009.

[34] Chun M. Chew, Radoljub I. Ristic, Robert D. Dennehy, James J. De Yoreo, "Crystallization of Paracetamol under Oscillatory Flow Crystallization of Paracetamol under Oscillatory Flow," *Crystal Growth & Design*, pp. 1045-1052, 2004.

[35] B. Ashraf Ali, M. Börner, M. Peglow, G. Janiga, A. Seidel-Morgenstern, D. Thévenin, "Coupled Computational Fluid Dynamics−Discrete Element Method Simulations of a Pilot-Scale Batch Crystallizer," *Crystal Growth & Design,* pp. 145-155, 2015.

[36] Welch, F. H. Harlow and J. E., "Numerical calculation of time-dependent viscous incompressible flow of fluid with free surface," *Physics of Fluids,* vol. 8, no. 12, p. 2182–2189, 1965.

[37] S. O. Unverdi, "A front-tracking method for viscous, incompressible multifluid flows," *Journal of Computational Physics*, vol. 100, no. 1, p. 25–37, 1992.

[38] Stanley Osher, James A Sethian, "Fronts propagating with curvature-dependent speed: Algorithms based on Hamilton-Jacobi formulations," *Journal of Computational Physics,* vol. 79, no. 1, p. 12–49, 1988.

[39] Sun, Mingyu, "Accuracy Improvement of PLIC-VOF Volume-Tracking Method Using the Equation of Surface Normal Vector," *Advances in Pure Mathematics,* vol. 3, pp. 219-225, 2013.

[40] G. H. Sauer, J. Schnerr, "Physical and Numerical Modeling of Unsteady Cavitation Dynamics," in *Fourth International Conference on Multiphase Flow*, New Orleans, USA., 2001.

[41] J. U. BRACKBILL, D. B. KOTHE, AND C. ZEMACH, "A Continuum Method for Modeling Surface Tension," *Journal of computational physics,* vol. 100, pp. 335- 354, 1992.

[42] D.J.E Harvie, M.R Davidson, M. Rudman, "An analysis of parasitic current generation in volume of fluid simulations," *Anzian Journal,* pp. 133-149, 2005.

[43] Wilcox, David C ., Turbulence Modeling for CFD, La Canada: DCW Industries, Inc., 2000.

[44] M. Sun, "Accuracy Improvement of PLIC-VOF Volume-Tracking Method Using the Equation of Surface Normal Vector," *Advances in Pure Mathematics,* pp. 219-225, 2013.

[45] K. Sangwal, "Effect of impurities on the metastable zone width of solute–solvent systems," *Journal of Crystal Growth,* p. 4050–4061, 2009.

[46] Nacera Amara, Berthe Ratsimba, Anne-Marie Wilhelm, Henri Delmas, "Crystalization of potash alum: effect of power ultrasound," *Ultrasonics sonochemistry*, pp. 265-270, 2001.

[47] P. Gonzalez-Contreras, J. Weijma , C. J. N. Buisman, "Bioscorodite Crystallization in an Airlift Reactor for Arsenic Removal," *Cryst. Growth Des,* p. 2699–2706, 2012.

[48] Sunil Mathew, Theo G. Keith Jr and Efstratios Nikolaidis, "Numerical simulation of traveling bubble cavitation," *International Journal of Numerical Methods for Heat & Fluid Flow,* pp. 393-416, 2006.